Materials Chemistry Horizons RESEARCH

Photocatalytic Degradation of Sumatriptan Succinate by ZnO, Fe Doped ZnO and TiO_2-ZnO Nanocatalysts

Elahe Alizadeh & Hadi Baseri*

School of Chemistry, Damghan University, Damghan 36716-45667, I.R. Iran

Corresponding author: Baseri@du.ac.ir & hadi.bass@yahoo.com (H. Baseri)

Mater. Chem. Horizons, 2022, 1(1), 7-21 10.22128/mch.2022.534.1002 OPEN ACCESS

ABSTRACT

Pharmaceutical pollutants are toxic trace components in the natural environment. In this work, removing Sumatriptan Succinate from the contaminated water by photocatalytic degradation reaction was investigated. Nanoparticles of ZnO, Fe (0.01 and 0.05) doped ZnO and TiO_2-ZnO composites were constructed by the co-precipitation method and characterized by FTIR, XRD, XRF, TGA, FE-SEM, BET-BJH, and UV-Vis spectroscopy methods. Then, the effects of various operating parameters of reaction temperature (10 to 80°C), reaction time (15 to 60 min), pH of the solution (4-11), the concentration of pharmaceutical pollutant (8 to 25 $\times 10^{-6}$ M), a dose of nanocatalysts (0.8 to 4.5 mg) and the stability or reusability of produced nanocatalysts on the degradation efficiency were studied. Based on the reported results, maximum degradation efficiency is about 70% for Fe (0.05) doped ZnO with 60 min reaction time, 1.5 mg catalyst weight, and contaminating concentration of 8×10^{-6} M.

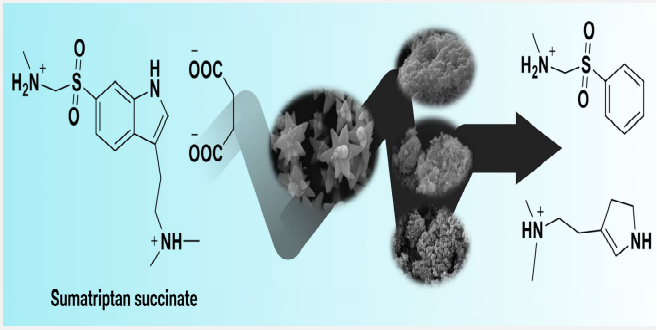

Keywords: Photocatalytic degradation, sumatriptan Succinate, ZnO, Fe doped ZnO, TiO_2, nanocatalysts

1. Introduction

Water pollution is one of the serious ecological threats we face today. With the growth of the human population and the development of various industries, the water pollution problem increases. Among these pollutions, pharmaceutical residues in the wastewaters are known as "emerging contaminants" and they significantly affect the environment and wildlife [1-4]. Therefore, their removal is of great importance.

Pharmaceutical residues enter the environment in several ways, such as research activity, hospital waste, animal waste, and expired medicine [5]. Different methods have been done for removing pharmaceuticals from the aquatic environments, such as biological processes [6,7], chemical adsorption by nano adsorbents [8, 9], and catalytic reactions [10-12].

Various elements and materials like aluminum, iron, titanium dioxide, clays, and silica have been used as catalysts on the nanoscale for many years [13]. The large surface area of nanoparticles has a positive effect on the reaction rate and it may be a reasonable explanation for their good catalytic activity. Metal oxide nanoparticles are very important and useful particles in environmental remediation [15]. Among them, nano zinc oxide (ZnO) is one of the most important and usable nanoparticles. It is a special material with a wide band gap (3.37 eV) that displays semiconducting and piezoelectric dual properties [15]. ZnO nanoparticles can be synthesized with different methods, such as: co-precipitation [16], sol-gel [17], microwave [18], sonochemical [19], vapor phase [20] and hydrothermal methods [21]. Doping a catalyst with suitable material and coupling two semi-conductors can enhance its catalytic performance. Therefore, the catalytic activities of doped catalysts were tested by researchers in many processes [22].

Received: May 08, 2022
Received in revised: May 28, 2022
Accepted: June 09, 2022

Sumatriptan Succinate (STS) is an effective drug for ending or relieving the intensity of migraine and cluster headaches [23]. From a chemical aspect, it is a butanedioic acid; 1-[3-[2-(dimethyl amino) ethyl]-1H-indol-5-yl]-N-methyl methane sulfonamide [23], and the removal of this pharmaceutical component is important, because it has a relatively high solubility in water.

Destroying STS with the forced degradation method in various conditions such as alkali degradation, acid degradation, oxidative degradation, and thermal degradation, is an effective removing method that was used by researchers [24]. In this work, ZnO was incorporated as a nanocatalyst for the degradation of STS under different conditions, and the effects of various factors such as the initial concentration of STS, amount of nanocatalyst, pH of the solution, the temperature of the solution, and time of visible light irradiation were studied on the degradation of STS.

The study targeted for removal of STS as a model component of pharmaceutical impurity. ZnO, Fe doped ZnO ([$Fe_xZn_{1-x}O$ (x=1% and 5%)]) and ZnO-TiO_2 nanocatalysts were synthesized successfully and they were characterized using XRD, XRF, FT-IR, FE-SEM, BET, and BJH methods. Adsorption/desorption isotherm and the adsorption spectra of nanocatalysts were studied and the effects of different parameters for the degradation of STS by the produced nanocatalysts were examined. Based on the reported results, Fe (5%) doped ZnO shows the best catalyst with degradation efficiencies higher than 70%.

2. Experimental

2.1. Materials

All chemicals were of analytical grade and used without further purification. STS ($C_{18}H_{27}N_3O_6S$, 99.73%) were purchased from Damavand daroo Company (Damghan, Iran). Zinc nitrate hexahydrate ($Zn(NO_3)_2.6H_2O$, 99%), Sodium hydroxide (NaOH, 99%), Titanium isopropoxide (TTIP) ($C_{12}H_{28}O_4Ti$, 97%), and Hydrochloric acid (HCl, 37%) were purchased from Merck Company (Germany). Iron (II) sulfate heptahydrate ($FeSO_4.7H_2O$, 99%) was purchased from Fluka Company (Germany). Sodium carbonate (Na_2CO_3, 99%) was purchased from Sinchem Chemical Company (South Korea). Ethanol (C_2H_5OH, 99.5%) and diethyl ether ($C_4H_{10}O$, 99%) were purchased from Scharlau Company (Spain). Deionized double distilled water was used for the preparation of nanocatalysts.

2.2. Instrumentation

The FTIR spectra of the adsorbent materials were taken with the Perkin Elmer RXI model operating at 400–4000 cm^{-1} in transmission mode. X-ray diffraction (XRD) patterns of samples were examined using D8-Advance, Bruker AXS (Cu K α1 (λ= 1.54064 Å)) model in the 2θ range of 10 to 80 degrees. The weight percent of the elements in the synthesized nanocatalysts was determined by XRF analysis (Bruker AXS S4). The BEL SORP mini and Finetec device were used for BET and BJH theory. The size and morphology of the nanoparticles were determined by Field Emission Scanning Electron Microscopy (HITACHI S-4160). UV-Vis Spectroscopy was used to determination of STS concentration in an aqueous solution (lambda 25). Separating of nanoparticles from the solute is conducted by centrifuging (SE.148). The pH of the solutions was measured with a Metrohm pH meter (728 pH lab). A mercury vapor pressure lamp (250 W) is used as the light source.

2.3. Preparation of nanocatalyst

2.3.1. Synthesis of nano ZnO

For the synthesis of ZnO nanoparticles, 0.3 g $Zn(NO_3)_2.6H_2O$ dissolved in 100 mL of deionized double distilled water with continuous stirring (Solution A), Then NaOH solution (NaOH 1M) was added to the solution (A) slowly (drop by drop) until the pH of the solution became 12. The white particles were washed three times with deionized double distilled water. Then it dried for 26 h at 90˚C in an oven. After drying, the resulting white precipitate was calcined at 500˚C for 1 h to obtain nanoparticles with high crystalline quality [25].

2.3.2. Synthesis of Fe doped ZnO, [$Fe_xZn_{1-x}O$ (x=1% and 5%)]

For the synthesis of Fe doped ZnO, stoichiometric quantities of $Zn(NO_3)_2.6H_2O$ and $FeSO_4.7H_2O$, dissolved in 100 mL deionized double distilled water (solution A) and then separately, solution B was prepared by dissolving specified amount of NaOH and Na_2CO_3 in deionized double distilled water. Solution (A) was heated to 80˚C and then the solution (B) was added slowly (drop by drop) to the solution (A) with continuous stirring and it refluxed for 1 h at the same temperature (80˚C). The resulting mixture was cold at laboratory temperature and washed three times with deionized double distilled water. These particles dried under vacuum at 50˚C for 14 h. The orange precipitate was calcined at 450˚C for 90 min.

2.3.3. Synthesis of nano ZnO-TiO_2

The TTIP was added to ethanol drop by drop and stirred for 30 minutes to achieve a yellow transparent sol at room temperature. The HCl solution (0.1 M) was added dropwise to the mixture and vigorously stirred for 2 hours. The HCl was used to control the rate of condensation and prevent fast gelation of the sol in this process [26]. On the other hand, $Zn(NO_3)_2.6H_2O$ was dissolved in ethanol and stirred for 1 hour. The prepared ZnO sol was added directly to the TiO_2 sol. After that, the solution was continuously stirred for 2 hours. The obtained gel was dried in an oven at 60°C for 20 hours and 110°C for 2 hours. Finally, the yellow precipitate was calcined at 400°C for 3 hours.

2.4. Procedures

For STS degradation experiments, 1.5 mg of nanocatalyst was added to 25 mL of STS solution (8×10^{-6} M) and shacked for 3 h (rpm was 250) in desired reaction conditions such as room temperature and neutral pH. Intended nanoparticles were separated from the aqueous solution by using a centrifuge after the completion of 3 h. The concentration of STS in aqueous solution was scanned in the spectrum mode from 200 to 400 nm and the overlain UV spectra were measured [27]. The degradation efficiency was calculated according to the following equation:

$$Degradation\ efficiency\ \% = \frac{(C_0 - C_t)}{C_0} \times 100 \quad (1)$$

Where C_0 and C_t are the initial and terminal concentrations of STS in the solutions, respectively. Moreover, for each experimental set, calibration curves were plotted to determine the concentration.

3. Results and discussion

3.1. Characterization of nanocatalysts

3.1.1. FTIR analysis

FTIR patterns of ZnO, Fe (0.01) doped ZnO, Fe (0.05) doped ZnO, and ZnO- TiO_2 are depicted in **Figure 1**. The spectra of synthesis nanocatalysts are the same and several well-defined bands at 490, 1120, 1388 and 3458 cm^{-1} become manifest in the FTIR spectrum and these peaks are consistent with similar articles [28, 29]. The peak at 490 cm^{-1} is due to metal oxygen modes and therefore, shows the formation of ZnO, Fe doped ZnO, and ZnO- TiO_2. The wide absorption peak of about 3458 and 1120 cm^{-1} are owing to the O-H stretching vibration of water or alcohols in synthesis nanocatalysts. The sharp peak of about 1388 cm^{-1} is due to H-O-H banding vibration, which can be assigned to the small amount of H_2O in ZnO nanocatalysts [30, 31].

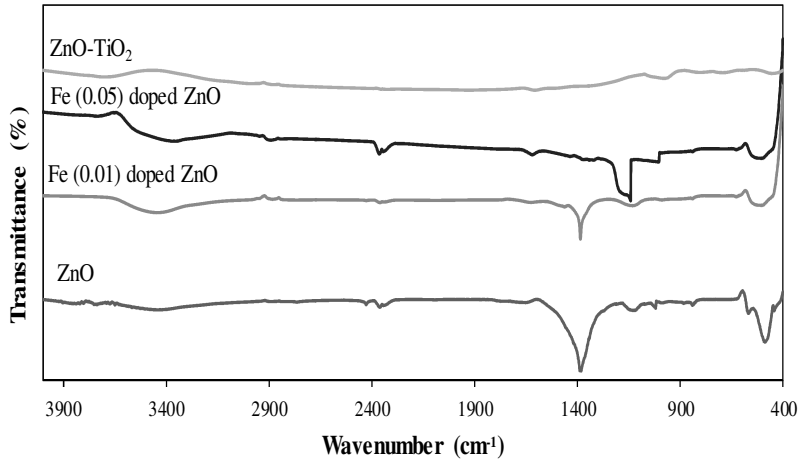

Figure 1. FT-IR spectra for nanoparticles of ZnO, Fe (0.01) doped ZnO, Fe (0.05) doped ZnO, and ZnO-TiO_2.

3.1.2. XRD analysis

The crystalline structures of the synthesized nanocatalysts recognize with XRD patterns (**Figure 2**). The patterns of samples are closely the same without any impurity peak. Sharp peaks with 2θ values of 31.8, 34.59, 36.35, 47.63, 56.63, 62.93, and 68.11° are observed for ZnO nanoparticles and the patterns of the three samples are relatively the same. These peaks are in good agreement with those of JCPDS card no. 36-1451. The additional peaks at about 68 and 69° show the presence of Fe atoms in the crystal structure of particles.

The crystallite sizes of the catalysts are calculated using Scherrer's formula (Eq.2) [25]:

$$D=\frac{K\lambda}{\beta\cos\theta} \qquad (2)$$

Where D is taken as the average crystallite size, λ is 1.5406 A˚, K is a constant equal to 0.9, β is the full width at half maximum (FWHM) in radians on the 2θ scale and θ is Bragg's angle for the diffraction peaks. According to the above equation, the average size of the crystallites for nanoparticles of ZnO, Fe (0.01) doped ZnO, Fe (0.05) doped ZnO, and ZnO- TiO_2 are reported in **Table 1**. By doping Fe metal cations, the mean crystallite size of particles is decreased and they are distributed homogeneously along the whole crystal [32, 33].

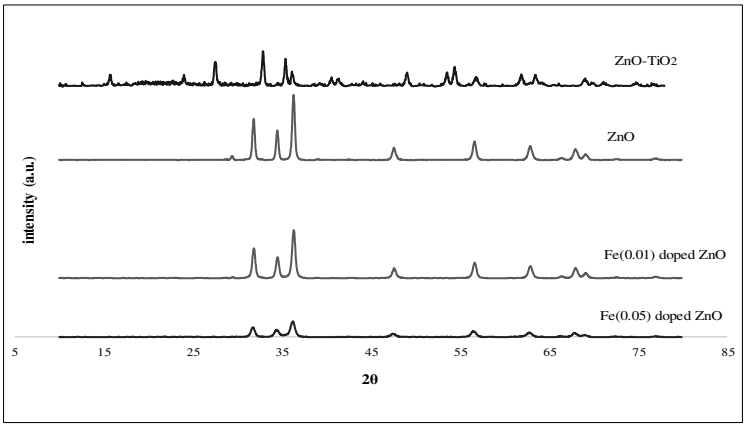

Figure 2. XRD patterns for nanoparticles of ZnO, Fe (0.01) doped ZnO, Fe (0.05) doped ZnO, and ZnO-TiO_2.

Table 1. Crystallite size of synthesized samples.

Sample	ZnO	Fe(0.01) doped ZnO	Fe(0.05) doped ZnO	ZnO-TiO_2
Crystallite size (nm)	26.29	21.03	23.38	26.08

3.1.3. XRF analysis

The weight percent of the elements in synthesized nanocatalysts is shown in **Table 2**. According to expectations, the nanoparticles with relatively high purities are performed.

Table 2. The weight percent of the elements in synthesized nanoparticles.

Elements	ZnO	Fe(0.01) doped ZnO	Fe(0.05) doped ZnO	ZnO-TiO_2
S	0.18	0.39	0.14	0.20
Si	0.07	0.02	0.09	0.09
Cl	-	0.10	0.05	0.87
Al	-	-	0.02	0.08
Zn	99.74	96.10	88.51	66.50
Fe	-	3.32	11.24	-
Ti	-	-	-	31.88

3.1.4. TGA analysis

TGA and DTA of nanoparticles are shown in **Figure 3**. All of the analyses were carried out in atmospheric air, with temperatures ranging from 20 to 600°C and at the rate of 10°C/min. As can be seen, all synthesized nanocatalysts have high thermal stability. TGA curves of the nanoparticles show weight losses below 150 ºC, which can be attributed to the loss of adsorbed water in the samples. The weight loss in the temperature range of 300 to 350ºC is attributed to the decomposition of $Zn(OH)_2$ in samples. The DTA curve has an exothermic peak at that temperature which may be attributed to the fact that volatile organic components generated by the dissociation of precursors react with O_2 to form CO_2 and H_2O. This is confirmed by the weight loss observed in the temperature region of 400–600°C in the TGA curve.

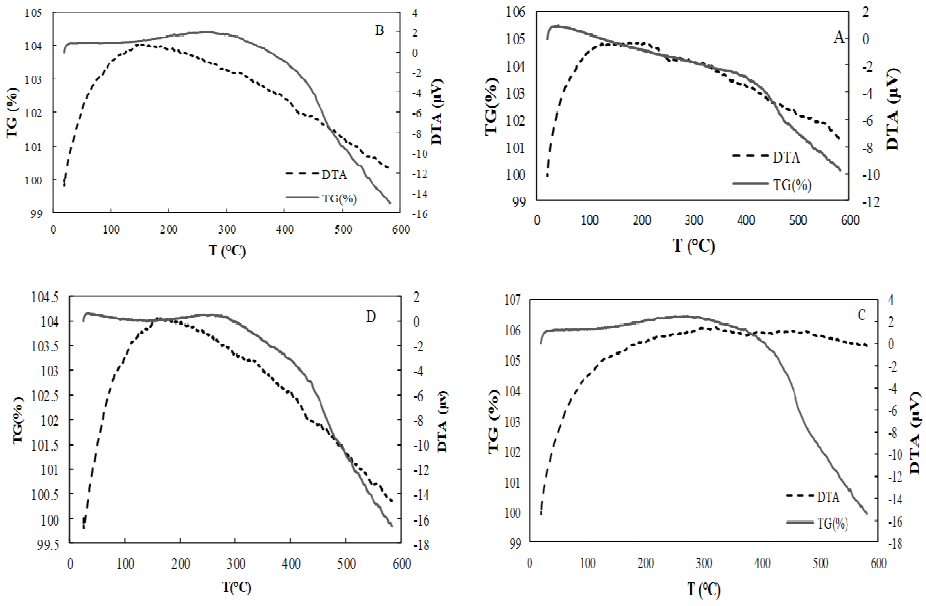

Figure 3. TGA/DTA curve of **(A)** ZnO, **(B)** Fe (0.01) doped ZnO, **(C)** Fe (0.05) doped ZnO and **(D)** ZnO-TiO_2 nanoparticles.

3.1.5. FESEM analysis

FESEM images of ZnO, Fe (0.01) doped ZnO, Fe (0.05) doped ZnO, and ZnO- TiO_2 nanoparticles are shown in **Figure 4**. The morphologies of Fe (0.01) doped ZnO, Fe (0.05) doped ZnO, and ZnO- TiO_2 particles are compact in comparison with pure ZnO particles. As can be seen, ZnO nanoparticles are flower-shaped but the other synthesized nanoparticles are relatively spherical. The average area and diameter of the obtained nanoparticles are reported in **Table 3**.

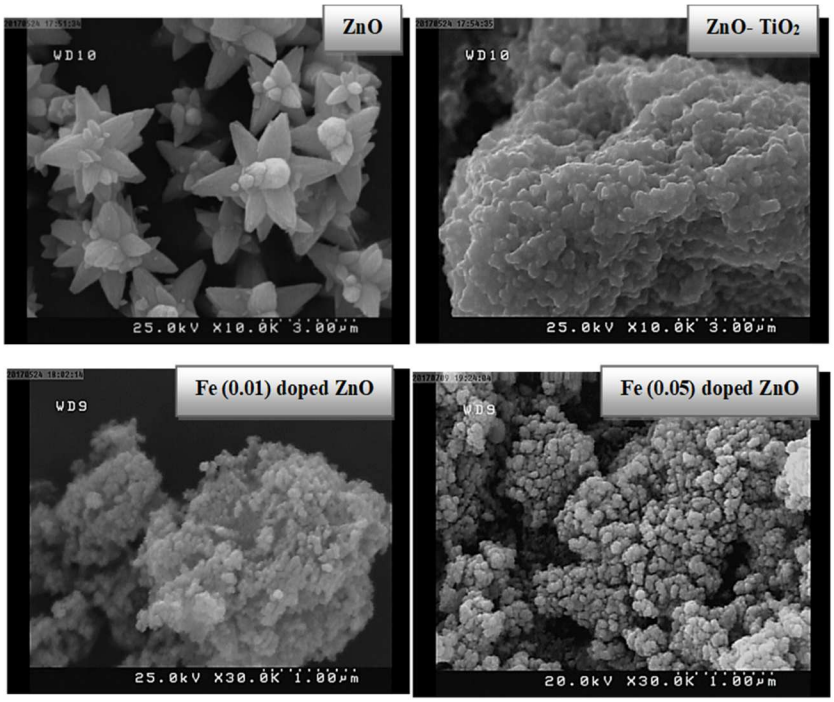

Figure 4. FE-SEM images of nanoparticles synthesized.

Table 3. Area and diameter of the synthesized nanoparticles.

Sample	Average area (nm^2)	Average diameter (nm)
ZnO	8015.291	101.05
Fe(0.01) doped ZnO	4004.739	71.43
Fe(0.05) doped ZnO	837.689	32.67
ZnO-TiO_2	7247.262	96.08

Particle size distribution histograms of the produced particles are presented in **Figure 5**. As shown in these figures, the mean sizes of the synthesized particles are about 70 nm. It can be seen that the presence of a small part of a different metal oxide has a characteristic effect on the particle size of the sample [34].

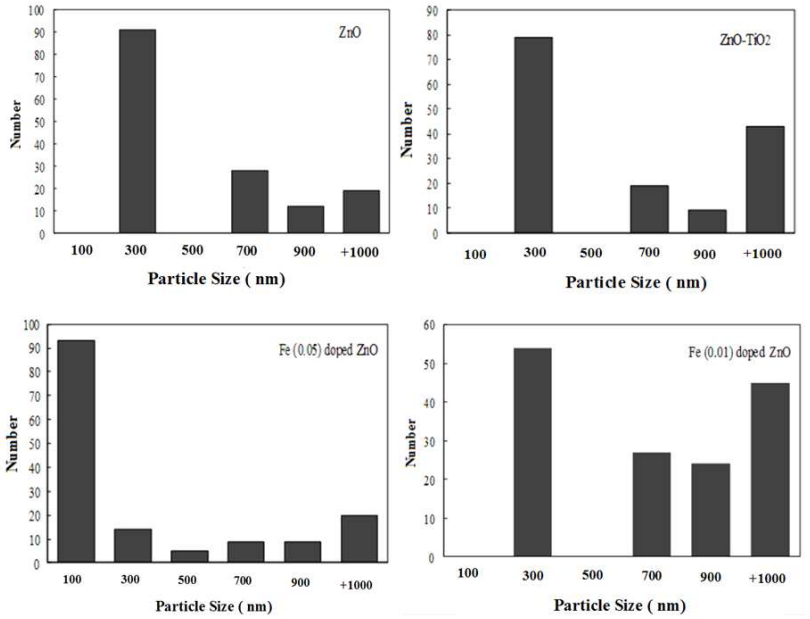

Figure 5. Obtained histogram from FE-SEM images for nanoparticles of ZnO, Fe (0.01) doped ZnO, Fe (0.05) doped ZnO-TiO_2.

3.1.6. Adsorption isotherm

Figure 6 shows the nitrogen adsorption-desorption isotherm of Fe (0.01) doped ZnO. These nanoparticles exhibit a type IV isotherm with an H_3-type hysteresis loop [35, 36]. This shape is seen in particles that have a track or cylindrical cavities. Specific surface area and porosity of synthesized Fe (0.01) doped ZnO were investigated by Brunaur-Emmett-Teller (BET) analysis. The results are shown in **Figure 7**. Using this figure, the single-layer capacity, surface area, total pore volume, and diameter of the mean pores can be calculated. **Table 4** shows the results of the BET analysis. The pore size distribution for Fe (0.01) doped ZnO shows in the BJH (Brunauer-Joyner-Halenda) curve (**Figure 8**). As can be shown in this curve, Fe (0.01) doped ZnO has a mesoporous structure with a relatively wide pore size distribution.

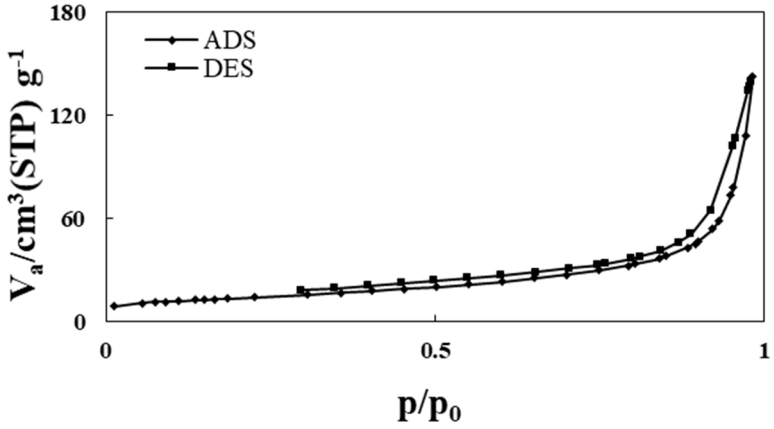

Figure 6. Nitrogen adsorption-desorption isotherms of Fe (0.01) doped ZnO.

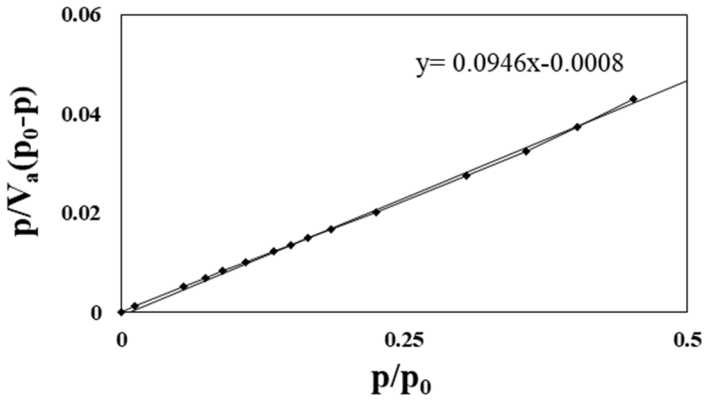

Figure 7. BET plot of Fe doped ZnO.

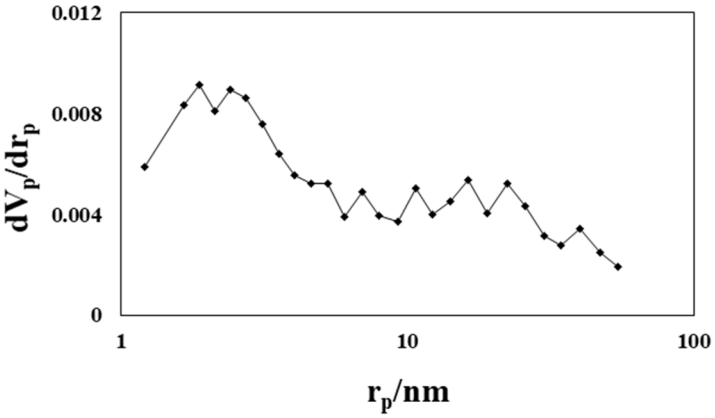

Figure 8. The BJH pore-size distribution of Fe doped ZnO.

Table 4. Results obtained from BET analysis for Fe (0.01) doped ZnO

Single-layer capacity (V_m (cm^3g^{-1}))	Surface area (BET) (m^2g^{-1})	Total pore volume (V_t (cm^3g^{-1}))	Diameter of the mean pores (nm)
10.658	46.389	0.2203	18.998

3.1.7. Investigation of optical properties of nanoparticles

The optical properties of synthesized nanoparticles are investigated using UV-Vis spectrometry and the obtained result is shown in **Figure 9**. The energy of the band gap for all samples was calculated by Eq. (3):

$$Eg = \frac{hc}{\lambda} \quad (3)$$

Where h is the Planck constant (h= 4.14 ×10^{-15} eV. s), c is the speed of light (c=2.99 × 10^8 m/s) and λ is the wavelength of light. The energy band gap calculated from the Planck equation for synthesized nanoparticles is presented in **Table 5**. The results show that the wavelength increases due to doping of zinc oxide with Fe, and by mixing this compound with TiO_2. It is predicted that by decreasing the band gap, the catalytic activity is increased. The reduction of band gap by transition metal ions doping is due to the strong p-d mixing of O atom and metal ions [37].

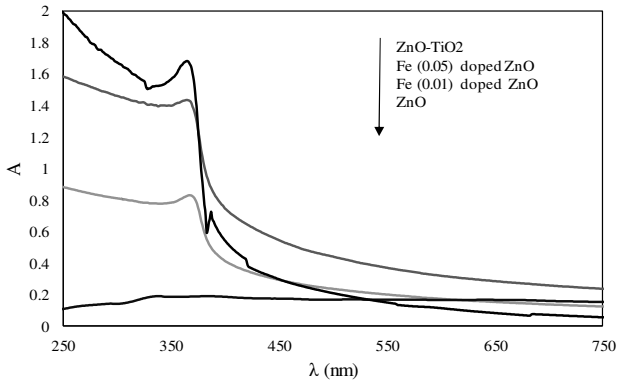

Figure 9. UV-Vis diffuses reflectance spectra.

Table 5. The band gaps and wavelength of synthesized nanoparticles.

Sample	Wavelength (nm)	Band gap (eV)
ZnO	338	3.66
Fe(0.01) doped ZnO	368	3.36
Fe(0.05) doped ZnO	364	3.40
ZnO-TiO_2	365	3.39

3.2. Degradation reaction

Pharmaceuticals, pesticides, and cosmetic products are usually found in wastewater. These compounds were destroyed hardly and they were never removed completely. Several processes have been performed for removing pharmaceutical components from the wastewater, but these methods are not efficient because the final degradation is low, expensive, and time-consuming. Therefore, innovative processes are required to save energy and have safer operations while avoiding the use of organic solvents [38]. Nanocatalyst destroying reactions are the most important methods for removing these pollutants [34]. In this research, degradation of Sumatriptan Succinate (STS) using ZnO-based nanoparticles was evaluated and the effect of some important parameters, e.g. initial concentration, nanocatalysts dose, pH of the solution, the temperature of the solution, and the time of visible light irradiation on degradation efficiency was investigated. The destruction amount was determined by UV-Vis spectroscopy and finally, the amount of recovery of nanocatalysts was evaluated.

3.2.1. Effect of initial concentration

Figure 10 shows the effect of initial concentration on the removal of STS from the aqueous solution. As can be shown, the highest degradation is observed in Fe (0.05) doped ZnO and STS concentration of 8×10^{-6} M, which is 17.16%. This concentration was selected for further studies. Based on the results reported in this figure, by increasing STS concentration degradation efficiency is decreased, because the catalyst activity is reduced by increasing the adsorbed compounds on the surface of the catalyst. The same effect was reported by Benhebal and his coworkers [39].

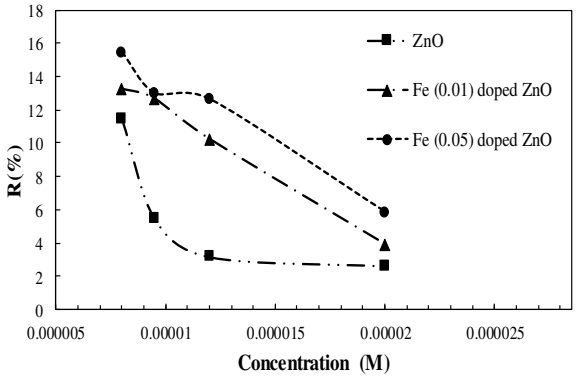

Figure 10. Effect of initial concentration on the removal of STS (nanocatalysts dose: 1.5 mg, contact time: 3 h, in-room temperature).

3.2.2. Effect of nanocatalyst dose

Various amounts of catalyst have been investigated for STS degradation and the results are shown in **Figure 11**. The percentage of degradation decreases with increasing the weight of the used catalyst. Based on the experimental results, 1.5 mg of nanocatalyst shows the best degradation efficacy in comparison with other values. This result can be attributed to the accumulation of catalysts in high amounts, which limits the number of active sites at the nanocatalyst's surface [40]. Therefore, 1.5 mg was selected as the optimum dose of catalyst in other experiments. Moreover, Fe (0.05) doped ZnO shows the best catalyst activity and in all other cases, this type of catalyst is selected.

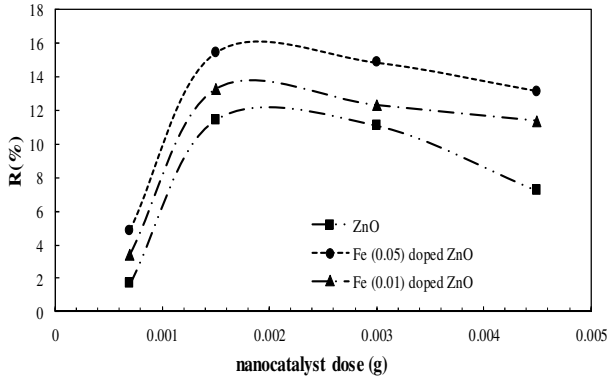

Figure 11. Effect of nanocatalysts dose on the removal of STS (initial concentration: 8×10^{-6} M with 3h contact time).

3.2.3. Effect of temperature

Temperature is one of the most important factors affecting the rate of chemical reactions. In many reactions, the reaction rate may be several times higher in high temperatures. Many studies have been conducted on the thermal degradation of drugs with degradation efficiency between 1% and 30% [41]. **Figure 12** shows the effect of temperature on the degradation of STS. According to the reported results, in the presence of all three nanocatalysts, an increase in the reaction temperature leads to an increase in the degradation efficiency, moreover, Fe (0.05) doped ZnO is the best nanocatalyst in all measured temperatures.

As mentioned in the literature [42], by increasing temperature, the rate of degradation reaction increased and it leads to an increase in degradation efficiency for STS components.

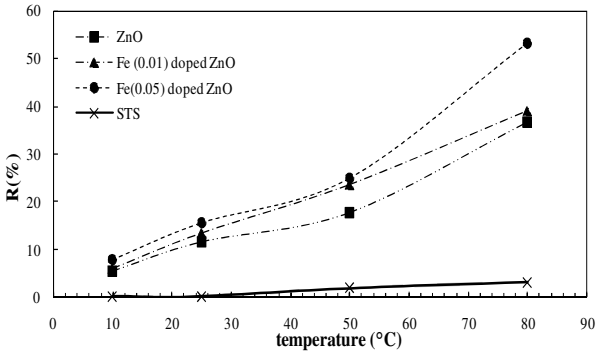

Figure 12. Effect of temperature on the removal of STS (initial conc.:8×10^{-6} M, dose of nanocatalysts: 1.5 mg, contact time: 3 h).

3.2.4. Effect of pH

Hydrolysis is one of the most common reactions that lead to the destruction of pharmaceutical substances and it is occurring within a different range of pH. Hydrolysis is a chemical process that results in chemical decomposition during the reaction with water. Hydrolysis involves the nucleophilic addition of water to the protonated compounds that can be ionized in acidic and alkaline conditions [43, 44]. The effect of pH on the removal of STS has been investigated in presence of nanocatalysts and the results are shown in **Figure 13**. According to the reported results, the degradation rate of STS in the alkaline condition is more than in the acidic condition in the absence and presence of different nanocatalysts. This can be attributed to the stability of the created compounds at high pH. In this section, Fe (0.05) doped ZnO is the best nanocatalyst in all measured values of pH.

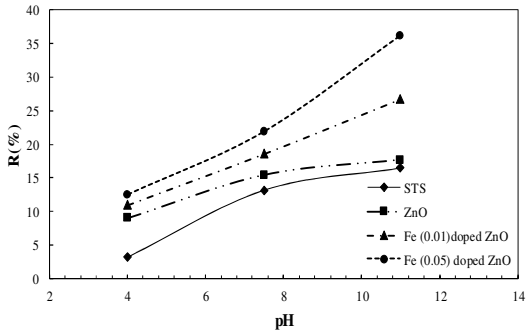

Figure 13. Effect of pH on the removal of STS (initial conc.: 8×10^{-6} M, a dose of nanocatalysts: 1.5 mg, contact time: 3 h, at room temperature).

3.2.5. The effect of time of visible light irradiation

In this section, the photocatalytic degradation of STS tested and the effects of light irradiation for the removal of STS are examined. A mercury vapor pressure lamp (250 W) is used as the light source. This commercially cheap light source emits about 80% visible light and 20% UVA radiation. The samples were located about 30 cm from the light source with continuous stirring. In this section, ZnO- TiO_2 nanocatalysts were also used, because TiO_2 is a very famous photocatalyst. The obtained results are shown in **Figure 14**. As can be seen from this figure, the degradation of the drug increased with increasing irradiation time. Another cause of degradation is the use of semiconductor nanocatalysts. When the light excites the band gap, the charge separation occurs in semiconductor nanoparticles. The maximum removal efficiency of about 70% was obtained in 60 min of light irradiation time and the present Fe (0.05) doped ZnO nanocatalyst.

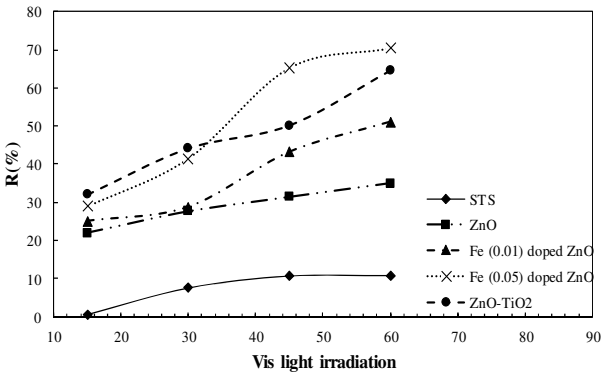

Figure 14. The effect of time of visible light irradiation on the removal of STS (initial conc.: 8×10^{-6} M, a dose of nanocatalysts: 1.5 mg).

3.3. Stability and reusability of nanocatalysts

In this section, the initial concentration of STS was 8×10^{-6} M, a dose of nanocatalyst was 3 mg, and samples were exposed to visible light for 60 min. The synthesis nanoparticles are separated from the aqueous solution by centrifuging after the completion of the reaction, and then they are washed with diethyl ether and dried at room temperature. To measure the reusability of nanocatalysts, the reaction is replicated four times. The obtained results are shown in **Figure 15**. As can be seen from this figure, due to better retrieval of active sites, Fe (0.01) doped ZnO is the best nanocatalyst instability.

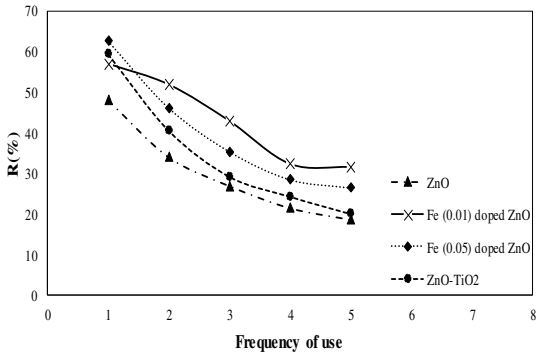

Figure 15. Chart of the recovery rate of synthesized nanocatalysts.

4. Conclusion

Nowadays, with the development of various industries, the water pollution problem increased rapidly, and specifically, the treatment of pharmaceutical residues from the wastewaters is an important concern. In this work, the degradation of Sumatriptan Succinate by the photocatalytic reaction is studied. Nanoparticles of ZnO, Fe (0.01 & 0.05) doped ZnO and TiO_2-ZnO composites are constructed by the co-precipitation method, and the effects of various operating parameters on the degradation efficiency are studied. Based on the reported results, photocatalytic degradation is an efficient method for removing STS from contaminated water. Fe (0.05) doped ZnO shows a relatively better catalytic effect in comparison to three other studied nanocatalysts. Moreover, by decreasing the initial concentration of STS and by increasing the reaction temperature, reaction time, and pH of the solution the degradation efficiency increased. 1.5 mg of catalyst in 100 mL of 8×10^{-6} M STS-water solution is the optimum catalyst dose, which degradation efficiency riches to higher values (about 70%) in the studied range of parameters. A comparison between similar works for catalytic and photocatalytic degradation of pharmaceutical components by using different ZnO-based nanocatalysts is depicted in **Table 6**.

Table 6. A comparison between similar works for catalytic and photocatalytic degradation of pharmaceutical components using different ZnO-based nanocatalysts.

Type of catalyst	Poulltants	Degr. eff.(%)	Reference
Mn Fe_2O_4 /ZnO/CQDs	Gntamicin	69.1 %	[44]
Cu and Fe /ZnO	Amlodipine Besylate	90 %	[33]
ZnO/CdO	4-nitrophenol	5- 98%	[45]
$FeCl_2$ /ac/ZnO	tamoxifen	75%	[46]
Fe @TiO_2/ZnO	STS	70%	This work

Authors' contributions

All authors contributed to data analysis, drafting and revising of the paper and agreed to be responsible for all the aspects of this work.

Acknowledgments

The authors wish to acknowledge financial and spiritual support from Damghan University.

Declaration of competing interest

The authors declare no competing interest.

Funding

This paper received no external funding.

Data availability

Data will be made available on request.

References

[1] B. Marinho, L. Suhadolnik, B. Likozar, M. Hus, M. Ziva, M. Ceh, Photocatalytic, electrocatalytic and photoelectrocatalytic degradation of pharmaceuticals in aqueous media: Analytical methods, mechanisms, simulation, catalysts and reactors, J. Clean. Prod. 343 (2022) 131061.

[2] F. Zhao, S. Fang, Y. Gao, J. Bi, Removal of aqueous pharmaceutical by magnetically functionalized Zr-MOFs: adsorption Kinetics, Isotherms, and regeneration, J. Coll. Inter. Sci. 615 (2022) 876-886.

[3] A. Heidari, M.N. Lotfollahi, H. Baseri, Regeneration of activated carbon loaded with cyclohexane using supercritical carbon dioxide: experimental results and modeling, Chem. Eng. Technol. 36 (2013), 315-322.

[4] H. Baseri, A. Haghighi-Asl, M.N. Lotfollahi, Thermodynamic modeling of solid solubility in supercritical carbon dioxide: comparison between mixing rules, Chem. Ind. Chem. Eng. Q. 9 (2013) 389-398.

[5] B. Tiwari, B. Sellamuthu, Y. Ouarda, P. Drogui, R.D. Tyagi, G. Buelna, Review on fate and mechanism of removal of pharmaceutical pollutants from wastewater using biological approach, Bioresour. Technol. 224 (2016) 1–12.

[6] S. K. Behera, H. W. Kim, J. E. Oh, H. S. Park,Occurrence and removal of antibiotics, hormones and several other pharmaceuticals in wastewater treatment plants of the largest industrial city of Korea, Sci. Total Environ. 409 (2011) 4351-4360.

[7] M. Kim, P. Guerra, A. Shah, M. Parsa, M. Alaee, S. A. Smyth, Removal of pharmaceuticals and personal care products in a membrane bioreactor wastewater treatment plant,Water Sci. Technol. 69(2014) 2221-2229.

[8] A. Puga, M.M. Moreira, M. Pazos, S.A. Fiogueiredo, M.A. Sanroman, C.D. Matos, E. Rosales, Continuous adsorption studies of pharmaceuticals in multicomponent mixtures by agroforestry biochar, J. inviron. Chem. Eng. 10 (2022) 106977.

[9] I. Zielinska, P. Daniel, S. Maciej, Analysis of the adsorption of selected pharmaceuticals on a composite material PEBAX/GO, J. Water Proc. Eng. 44 (2021) 102272.

[10] D. Xia, W. Wang, R. Yin, Z. Jiang, T. An, G. Li, P. K. Wong, Enhanced photocatalytic inactivation of Escherichia coli by a novel Z-scheme g-C3N4/m-Bi2O4 hybrid photocatalyst under visible light: The role of reactive oxygen species, Appl. Catal. B. 214 (2017) 23-33.

[11] T. N. J. I. Edison, M. G. Sethuraman, Y. R. Lee, NaBH4 reduction of ortho and para-nitroaniline catalyzed by silver nanoparticles synthesized using Tamarindus indica seed coat extract, Res. Chem. Intermed. 42(2016) 713-724.
[12] M. Farzadkia, A. Esrafili, M. A. Baghapour, Y. D. Shahamat, N. Okhovat,Degradation of metronidazole in aqueous solution by nano-ZnO/UV photocatalytic process, Desalin. Water Treat. 52 (2014) 4947-4952.
[13] S. B. Singh, P. K. Tandon,Catalysis: a brief review on nano-catalyst, J. Energy. Chem. Eng. 2(2014) 106-115.
[14] M. M. Khan, S. F. Adil, A. Al-Mayouf,Metal oxides as photocatalysts, J. Saudi Chem. Soc. 19 (2015) 462-464.
[15] A.K. Zak, W.A. Majid, M.E. Abrishami, R. Yousefi, X-ray analysis of ZnO nanoparticles by Williamson-Hall and size-strain plot methods,Solid StateSci. 13 (2011) 251-256.
[16] A. B. Djurisic, A. M. C. Ng, X. Y. Chen, ZnO nanostructures for optoelectronics: material properties and device applications, Prog. Quant. Electron. 34 (2010) 191-259.
[17] J. N. Hasnidawani, H. N. Azlina, H. Norita, N. N. Bonnia, S. Ratim, E. S. Ali, Synthesis of ZnO nanostructures using sol-gel method, Procedia Chem. 19 (2016) 211-216.
[18] D. Sharma, S. Sharma, B.S. Kaith, J. Rajput, M. Kaur, Synthesis of ZnO nanoparticles using surfactant free in-air and microwave method,Appl. Surf. Sci. 257 (2011) 9661-9672.
[19] R. S. Yadav, P. Mishra, A. C. Pandey, Growth mechanism and optical property of ZnO nanoparticles synthesized by sonochemical method,Ultrason. Sonochem. 15 (2008) 863-868.
[20] L. E. Shi, Z. H. Li, W. Zheng, Y. F. Zhao, Y. F. Jin, Z. X. Tang, Synthesis, antibacterial activity, antibacterial mechanism and food applications of ZnO nanoparticles: a review, Food Addit. Contam. 31 (2014) 173-186.
[21] P. M. Aneesh, K. A. Vanaja, M. K. Jayaraj, Synthesis of ZnO nanoparticles by hydrothermal method, Nanophotonic Mater. 6639 (2007), 66390J-1.
[22] R.M. Mohamed, D.L. McKinney,W.M. Sigmund, Enhanced nanocatalysts, Mater. Sci. Eng. 73 (2012) 1-13.
[23] K. N. Prashanth, K. Basavaiah, C. M. Xavier, Development and validation of UV spectrophotometric methods for the determination of sumatriptan succinate in bulk and pharmaceutical dosage form and its degradation behavior under varied stress conditions, J. Assoc. Arab Univ. Basic Appl. Sci. 15(2014) 43-52.
[24] X. Xu, M. G. Bartlett, J. T. Stewart,Determination of degradation products of sumatriptan succinate using LC-MS and LC-MS-MS, J. Pharm. Biomed. Anal. 26(2001) 367-377.
[25] B.D. Cullity, S.R. Stock,Elements of X-ray Diffraction, third ed., Prentice Hall, New York, 2001.
[26] M.Jafari, S.Razavein, A. Saffar, Synthesis and characterization of TiO_2-ZnO-xAl2O3 Nano-composite, Proceedings, MONTRÉAL'2014 AES-ATEMA 17th Int. Conference, Montréal, Canada, (2014) 153–158.
[27] M. Sharma, C. Kothari, O. Sherikar, P. Mehta, Concurrent Estimation of Amlodipine Besylate, Hydrochlorothiazide and Valsartan by RP-HPLC, HPTLC and UV–Spectrophotometry, J. Chromatogr. Sci. 52 (2013) 27-35.
[28] Y. T. Prabhu, K. V. Rao, V. S. S. Kumar, B. S. Kumari, synthesis of ZnO nanoparticles by novel surfactant assisted amine combustion method,Adv. Nanopart. 2 (2013) 45-54.
[29] M. I. Khalil, M. M. Al-Qunaibit, A. M. Al-Zahem, J. P. Labis, Synthesis and characterization of ZnO nanoparticles by thermal decomposition of a curcumin zinc complex, Arabian J. Chem. 7 (2014) 1178-1184.
[30] A.J. Reddy, M.K. Kokila, H. Nagabhushan, R.P.S. Chakradhar, C. Shivakumar, J.L. Rao, B.M. Nagabhushan, Structural, optical and EPR studies on ZnO: Cu nanopowders prepared via low temperature solution combustion synthesis, J. Alloys Compd. 509 (2011) 5349–5355.
[31] R.A. Nyquist, R. Kagel, Infrared Spectra of Inorganic Compounds, Academic Press, Inc., New York, London, 1971. p. 220.
[32] S. Tizro, H. Baseri, Heavy Metals Removal from Wastewater by Using Different Kinds of Magnetite Nano-Adsorbents: Effects of Different Organic and Inorganic Coatings on The Removal of Copper and Lead Ions, Adv. Mater. Process. 4(4) (2016) 15-29.
[33] E. Alizadeh, H. Baseri, Catalytic degradation of Amlodipine Besylate using ZnO, Cu doped ZnO, and Fe doped ZnO nanoparticles from an aqueous solution: Investigating the effect of different parameters on degradation efficiency, Solid State Sci. 78 (2018) 86-94.
[34] J. Singh, J. K. Yang, Y. Y. Chang, Rapid degradation of phenol by ultrasound-dispersed nano-metallic particles (NMPs) in the presence of hydrogen peroxide: A possible mechanism for phenol degradation in water, J Environ Manage. 175 (2016) 60-66.
[35] B. Thokchom, P. Qiu, M. Cui, B. Park, A. B. Pandit, J. Khim, Magnetic Pd@ Fe_3O_4 composite nanostructure as recoverable catalyst for sonoelectrohybrid degradation of Ibuprofen, Ultrason. Sonochem.34 (2017) 262-272.
[36] Q. Yuan, W. Deng, Q. Zhang, Y. Wang, Osmium-Catalyzed Selective Oxidations of Methane and Ethane with Hydrogen Peroxide in Aqueous Medium, Adv. Synth. Catal. 349 (2007) 1199-1209.
[37] Y. Junejo, A. Güner, A. Baykal,Synthesis and characterization of amoxicillin derived silver nanoparticles: Its catalytic effect on degradation of some pharmaceutical antibiotics, Appl. Surf. Sci. 31 (2014) 914-922.

[38] H. Benhebal, M. Chaib, T. Salmon, J. Geens, A. Leonard, S. D. Lambert, B. Heinrichs, Photocatalytic degradation of phenol and benzoic acid using zinc oxide powders prepared by the sol–gel process, Alexandria Eng. J. 52 (2013) 517-523.
[39]Z. Ž. Stoiljković, M. B. Jadranin, S. L Đurić, S. D. Petrović, A. M. L. Ivić, D. Ž. Mijin, Investigation of forced and total degradation products of amlodipine besylate by liquid chromatography and liquid chromatography-mass spectrometry, Chem. Ind. Chem. Eng. Q. 20(2014) 295-304.
[40] N. Modirshahla, M. A. Behnajady,Photooxidative degradation of Malachite Green (MG) by UV/H_2O_2: Influence of operational parameters and kinetic modeling, Dyes Pigm. 70 (2006) 54-59.
[41] E. Shokati fard, H. Baseri, ZnO-based composite catalysts for photocatalytic degradation of reactive black 5, and the optimization of process parameters, Water. Environ. J. (2022) 1-14.
[42] M. R. D. P.Blessy, R. D. Patel, P. N. Prajapati, Y. K. Agrawal, Development of forced degradation and stability indicating studies of drugs—A review, J. Pharm. Anal. 4(2014) 159-165.
[43] D. Saxena, S. Damale, A. Joshi, A. Datar, Forced degradation studies of amlodipine besylate and characterization of its major degradation products by LC-MS/MS, Int. J. Life Sci. Biotechnol. Pharma Res. 3 (2014) 196-173.
[44] M. Rahal, Y. Atassi, I. Alghoraibi. Preparation of separable Mn Fe_2O_4/ZnO/CQDs as a visible light photocatalyst for Gentamicin treatment, Mater. Chem. Phys. 286 (2022) 126123.
[45] A.M. Mostafa, E.A. Mwafy, Synthesis of Zn/CdO thin film for catalytic degradation of 4-nitrophenol, J. Mol. Struct. 1221 (2020) 128872.
[46] N. Nasseh, M.T. Samadi, M. Ghadirian, A.H. Panahi, A.Rezaie, Photo-catalytic degradation of tamoxifen by using a novel synthesized magnetic nanocomposite of $FeCl_2$@ac@ZnO: A study on the pathway, modeling, and sensitivity analysis using artificial neural network (AAN), J. Environ. Chem. Eng. 10(3) (2022) 107450.